Ma, S., Li, T., Motagh, M., Auer, S., Liu, Y., Liu, J. (2024): Complex Scattering Mechanisms at Power Lines in X-Band SAR Imagery. - IEEE Geoscience and Remote Sensing Letters, 21, 4015805.

https://doi.org/10.1109/LGRS.2024.3452709

Complex scattering mechanisms at power lines in X-Band SAR imagery

Sijie Ma, *Student Member*, *IEEE*, Tao Li, Mahdi Motagh, Stefan Auer, *Member, IEEE*, Yan Liu, and Jie Liu

***Abstract*—The analysis of complex scattering patterns in SAR images of high-voltage power lines is important to comprehend the multi-reflection effects of these cylindrical shape structures. Such insights are invaluable for applications related to inspection management, particularly in safety analysis and ongoing monitoring. This paper introduces a novel point scattering tracing method to dissect the intricate multi-reflection effects of power lines in high-resolution X-band SAR data. The paths of multi-reflection events at the power lines are delineated through a proposed model, which leverages LiDAR point cloud data and SAR system parameters with subpixel precision. Under the condition of a parallel tangent line to the azimuth direction, the proposed quadratic polynomial model is solvable to pinpoint the centers of the single- and triple-reflection point signatures of power lines in SAR coordinate. Analysis of time series SAR images reveals the activation of the double- and triple-reflection effects induced by water ripples or swinging lines, which is challenging to quantify. The proposed mathematical model is validated through testing with TerraSAR-X data in two distinct cases, and the results are highly consistent. The new insights of both visible and invisible components of the double and triple reflections of power lines introduce new challenges to SAR research.**

***Index Terms*—SAR, geometric optics method, power lines, multi-reflection, creeping wave.**

I. INTRODUCTION

Identifying multi-reflection from power lines in high-resolution X-band space-borne SAR images is a distinctive challenge. In contrast to other artificial structures, the power line structure is explicit and can clearly depict the properties of multi-reflection. Its complexity arises from the centimeter-scale diameter, catenary shape and orientation of power lines.

Most studies focus on multi-reflection from large manmade structures such as bridges, the Eiffel Tower, ancient Egyptian pyramids and dams [1,2,3,4,5]. These structures display a distinctive but difficult-to-recognize multi-reflection effects on SAR images. Auer et al. [3] introduced a ray-tracing method to simulate multi-reflection based on geometric attributes to comprehend multi-reflection building structures. Lee et al. [1] encountered a similar challenge when examining the multi-reflection of two cables on a suspension bridge, which was the Great Belt Bridge in their study. The analysis revealed a three-order reflection from two cables, whose diameters were nearly 1 m. Notably, two curved- and one straight-line signatures were discerned against a sea background. The study demonstrated symmetry between single- and triple-reflections of the bridge cable and elucidated the intricate dynamics of double-reflection phenomena.

Limited attention has been dedicated to the point signatures of power lines in spaceborne SAR images. L. Yan et al. [6] first delved into this aspect by examining the point signatures in TerraSAR-X (TSX) SAR data. Point signatures are sensitive to the intersection angle between the line direction and the heading of the SAR sensors, which is the lateral incidence angle. A statistical approach in [7] quantified that this lateral incidence angle should not exceed 15° for the visibility of these spots. K. Sarabandi et al. [8] discovered periodic Bragg scattering in millimeter-band SAR. They reported that the signal energy notably decreased to more than 20 dB when the lateral incidence angle exceeded 15°. This value is consistent with the value derived from [7]. S. Shi et al. [9] used a physical optics (PO) method to simulate the radar cross section (RCS) of power lines across SAR sensors with X-, C-, L-, and P-band signals. The studies assumed that the sag point of power lines formed a point signature, and the RCS changed according to the lateral incidence angle.

Interestingly, the double- and triple- reflections of signals at oil tanks are similar to the power line point signature [10,11], where the point signatures' centers are located on the line of sight of the SAR sensor on the outside and inner wall of the tank. The creeping wave signal that propagates on a circular cylinder tends to decrease in linear energy [12,13].

In Section II, a point scattering tracing method based on the Geometrical Optics (GO) method is presented to demonstrate the multi-reflection of power lines. Section III introduces a quadratic polynomial model to simulate the center positions of single- and triple-point signatures in SAR coordinate. The discussion encompasses speculation and the creeping wave mechanism of the multi-reflection effects of power lines.

This work was sponsored by the National Natural Science Foundation of China (No. 42074031,41674032,41274048). *(Corresponding author: Tao Li).*

Sijie Ma, Tao Li and Jie Liu are with GNSS Research Centre, Wuhan University, Wuhan, 430079, China and also with School of Geodesy and Geomatics, Wuhan University, 129 Luoyu Road Wuhan, 430079, China (e-mail: sjma99@whu.edu.cn; TaoLi@whu.edu.cn; Liujie-INSAR@whu.edu.cn).

Yan Liu is with State Key Laboratory of Power Grid Environmental Protection, China Electric Power Research Institute, Wuhan, China. (e-mail: liuyan5@epri.sgcc.com.cn).

Mahdi Motagh is with Section of Remote Sensing and Geoinformatics, GFZ German Research Centre for Geosciences, Potsdam, 14473, Germany and also with institute of Photogrammetry and Geoinformation, Leibniz University Hannover, Hannover, 30167, Germany (e-mail: motagh@gfz-potsdam.de).

Stefan Auer is with Remote Sensing Technology Institute, German A erospace Center (DLR), Wessling, 82234, Germany (e-mail: stefan.auer@dlr.de).

Section IV uses two TSX datasets to demonstrate the proposed approach and explain the nature of signal reflection effects. The conclusion highlights the novelties of the approach and outlines future perspectives.

II. Point Scattering Tracing Method

Building upon the GO method, which was used to analyze nearly-1-m-diameter suspension bridge cables [1], this paper introduces a point scattering tracing method for 2~3-cm-diameter power line cylinder conductors. The goal is to formulate the single-, double-, and triple-reflection routes. Fig. 1 shows the geometric configuration of multi-reflection for a point on a power line in an oblique incident plane, which corresponds to the SAR range direction.

The red arrow shows the single-reflection route of the SAR signal at a specific point N_i on the power line, where N'_i is the corresponding single-reflection location in the SAR coordinate. Extending from point N_i to the water surface, the green line represents the double-reflection route of the SAR signal with an additional (R1+R2) length compared to the single reflection. N''_i is the double-reflection location. The purple line shows the extended 2*(R1+R2) distance of triple-reflection route point N_i in the range direction and serves as N'''_i to depict the triple-reflection location.

In SAR coordinate, the range of pixel numbers $S_{N'_iN''_i}$ between N'_i and the double-reflection point N''_i is:

$$S_{N'_iN''_i} = \frac{1}{2}\frac{(R1+R2)}{\delta_r} = \Delta h_{N_i} * \frac{\cos\eta}{\delta_r} \quad (1)$$

$$R1 = R2 * \cos 2\eta \quad (2)$$

$$R2 = \frac{\Delta h_{N_i}}{\cos\eta} \quad (3)$$

where Δh_{N_i} is the height difference between N_i and its water surface perpendicular to the foot point N_{ig}. R1 and R2 denote the additional SAR signal propagation routes in the range direction for double- and triple-reflection, and the single reflection of point N_i is a reference position in the range direction. η is the local incidence angle, and δ_r is the range resolution (m/pixel).

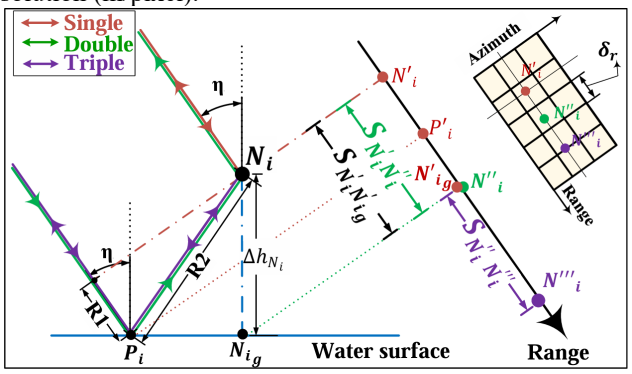

Fig. 1. Multi-reflection signal route of a point on a power line.

For the triple-reflection geometry, the range of pixel numbers $S_{N'_iN'''_i}$ between N'_i and triple-reflection point N'''_i is:

$$S_{N'_iN'''_i} = \frac{R1+R2}{\delta_r} = 2 * \Delta h_{N_i} * \frac{\cos\eta}{\delta_r} \quad (4)$$

N'_{ig} is the single-reflection point N_{ig} in the SAR coordinate. Notably, N'_{ig} coincides with the double-reflection point N''_i, i.e., despite the catenary of each power line, the double-reflection indefinitely persist as straight lines. The range pixel number of the single-, double- and triple-reflection of N_i is:

$$S_{N'_iN''_i} = S_{N''_iN'''_i} = S_{N'_iN'_{ig}} \quad (5)$$

III Powerline Multi-Reflection Mechanism

A. Line single and triple reflection spot simulation model

Fig. 2a shows a site photo of the power lines in Yezhihu Lake in Wuhan, China (YZH). Fig. 2b shows the TSX averaged image, which displays puzzling multi-reflection effects. The simulated multi-reflection effects are based on the model in Section II, which uses the LiDAR points (Fig. 2c) overlapped on the averaged SAR image, as shown in Fig. 2e.

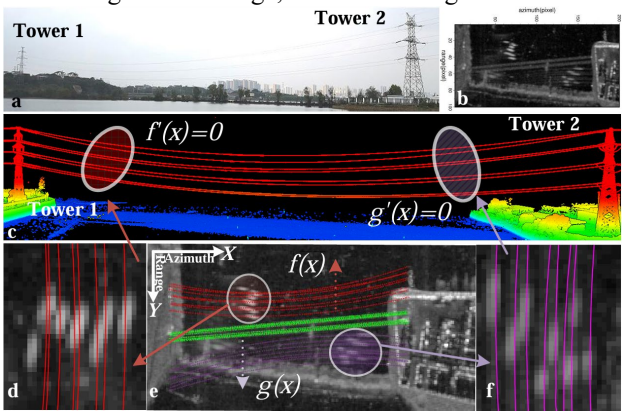

Fig. 2. Test site 1, Yezhihu, Wuhan, China. (a) Onsite photo; (b) averaged TSX image; (c) power line UAV LiDAR data; (d) single-reflection lines; (e) simulated single-, double- and triple-reflection lines on (b); (f) triple-reflection lines.

In Fig. 2e, the red lines represent the simulated single reflection of power lines using the LiDAR and SAR parameters and Range-Doppler equation. The green and purple lines correspond to the simulated double and triple reflection derived by (1)-(4), respectively. The line signatures simulated by single and triple reflection cannot be found in the averaged SAR images, whereas the double reflection is very clear. There are several bright point signatures precisely positioned along the simulated single- and triple-reflection lines, as shown in Figs. 2d and f. This finding suggests that single and triple reflections the from lines are responsible for these bright point signatures, but there may be an additional mechanism that concentrates the scattering into spots instead of lines as in double reflection. Furthermore, the single and triple point signatures are not located at the lowest parts of the power lines, as shown in Fig. 2e. They are located at different segments of the lines circled in Fig. 2c. In Figs. 2d and f, single- and triple-point signatures in the enlarged averaged SAR images overlap with the simulated lines derived from the LiDAR points of the power lines and (4).

Each point signature center is located at the lowest position of the curve in the range direction. Two quadratic polynomials are introduced to determine the point signature locations in the

SAR coordinate: $f(x)$ for the single reflection and $g(x)$ for the triple reflection:

$$f(x) = a_1x^2 + b_1x + c_1$$
$$g(x) = a_2x^2 + b_2x + c_2 \quad (6)$$

where a_1 and a_2 are quadratic coefficients; b_1 and b_2 are the primary term coefficients; c_1 and c_2 are constant terms. The azimuth is set as the X axis, and the range direction is set as the Y axis, as shown in Fig. 2e.

Previous studies on the reflection of power lines and cylindrical metal wall edges indicate that the lateral incidence angle to the power line is zero, and the specular reflection is the maximum [8,9,10,11]. According to (6), when those two quadratic polynomials have the lowest position in the azimuth direction, they will have a tangent line parallel to the azimuth direction as follows:

$$f'(x) = 2a_1x + b_1 = 0$$
$$g'(x) = 2a_2x + b_2 = 0 \quad (7)$$

The point signature centers of the single and triple reflections are on $f'(x) = 0$ and $g'(x) = 0$, respectively. If the quadratic polynomials do not have a tangent line between two towers, no point signature is visible.

B. SAR signal propagation on a power line

To reveal the intricate multi-reflection effects from power lines, the propagation route and speculation condition of the power line cylinder geometry must be considered.

Fig. 3 depicts the SAR signal that illuminates the power lines and water surface with complex propagation routes. The SAR signal illuminates the power lines in two directions: from the SAR sensor and from the water surface under specular reflection condition.

Fig. 3a depicts the direct illumination of the SAR signal on the power line, which results in specular reflection and an inverted creeping wave and forms a single reflection.

In Fig. 3b, the SAR signal propagation path is satellite-water-cable-satellite, and the reverse path is satellite-cable-water-satellite. In the double-reflection route, the SAR signal is not in a specular reflection on the power line, whereas the creeping wave condition is more reasonable. Moreover, the SAR signal propagation route in this case is more likely the bistatic SAR. The triple-reflection route (Fig. 3 c) of the power line is similar to single reflection, whereas the SAR signal illuminates the water surface.

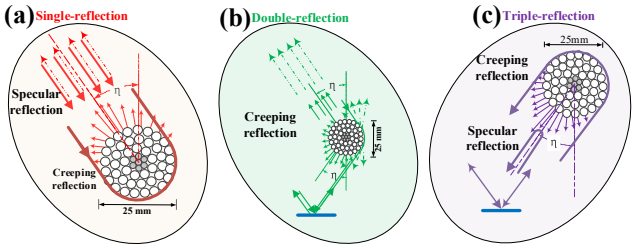

Fig. 3. SAR signal propagation route on the power line. (a) Single-reflection; (b) Double-reflection; (c) Triple-reflection.

C. Summary of signal multiple reflections

Fig. 4 depicts a 3D overview diagram in geographical coordinate to illustrate the SAR signal multi-reflection routes between power line and water surface. The red, green, and purple arrows represent the single-, double-, and triple-reflection routes, respectively. The single-reflection and triple-reflection point signatures are formed by two different line segments. With respect to geometrical coordinate, we do not have GO and PO models to define line segments that foster the single- and triple-reflection point signatures, which introduces new challenges to SAR research.

To schematically demonstrates the geometrical coordinate, the single-reflection point signature N_i is labeled on the power line with a foot point N_{ig} on the water surface. The water surface speculation point is on P_i, which forms a curved-line shape labeled as line P. Due to the one-to-one correspondence between the points on the power line and the simulated multi-reflection line, (6)-(7) and the Range-Doppler equation can help locate the 3D point signature on the power line in geographical coordinate.

Our proposed model demonstrates that changes in power line sag tension affect the quadratic polynomials in SAR coordinate. These slight changes in the polynomials, which are mainly caused by temperature, shift the point signatures in the azimuth and range directions, as reported in [7]. Once the catenary function of the power line has been derived, we can incorporate factors such as tension and material parameters and invert the line sag condition using daily SAR-acquired images.

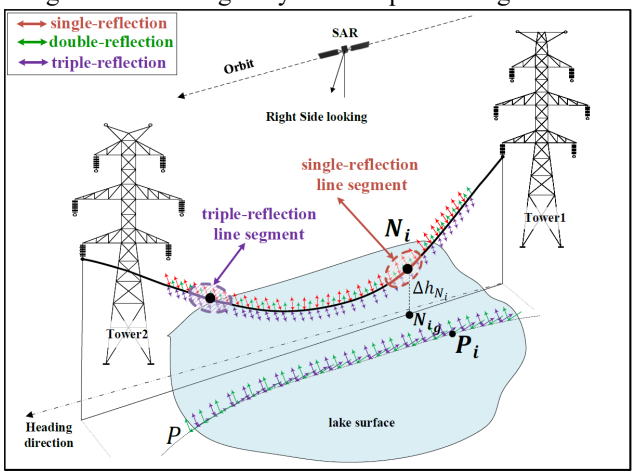

Fig. 4. 3D diagram of the SAR signal propagation.

IV. RESULTS

A. YZH (Wuhan China) case results

In the case of YZH (Fig. 2.a), the power lines extend to nearly 330 m and are suspended over the lake surface. From 2013 to 2018, 65 TSX-SAR strip-mode images were collected and co-registered with ground control points for subsequent analysis. To account for the intermittent disappearance of double- and triple-reflection effects, these datasets were categorized into three groups based on the frequency of multi-reflection occurrences.

In group I, which included 46% of the datasets, the single- and triple-point signatures are distinctly visible, whereas the double-reflection signature is imperceptible, as shown in Fig. 5a. A plausible assumption in this case is that the calm water

surface contributes to the stability and brightness of the triple-reflection point signatures. However, there is no reasonable assumption to account for the invisibility of double reflection.

In group II, the double reflection is distinctly visible, whereas the line texture of triple reflection is faint and challenging to identify, as shown in Fig. 5b. The triple-reflection point signatures are imperceptible. Consequently, the water surface roughness and ripple conditions in this group may differ from those in group I. The invisibility of triple-reflection point signatures indicates that the mechanism behind triple reflection is more intricate than that behind double reflection and potentially involves both the swinging conditions of the lines and water surface ripples.

In group III, which constitutes 22% of the datasets, both triple-reflection point signature and line texture are inexplicably discernible, as shown in Fig. 5c. Another distinction is that the line texture of the double-reflection mode appears slightly dimmer. The mechanism of this phenomenon remains unknown.

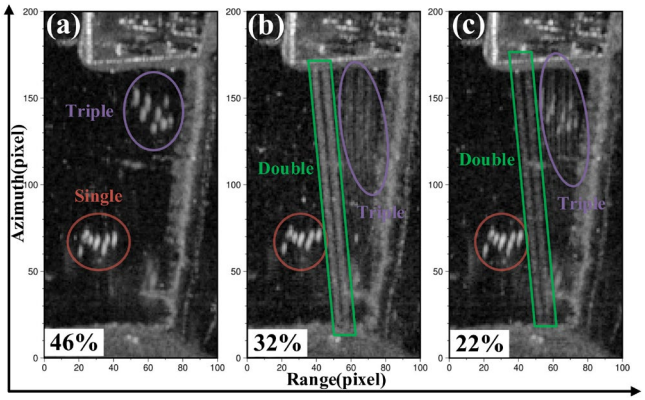

Fig. 5. Three groups of averaged SAR images (YZH). (a) Group I; (b) Group II; (c) Group III.

Fig. 6 shows the simulated single- and triple-reflection lines and point signatures on the averaged SAR image. The colored lines represent the simulated the reflections of the power lines, where various colors refer to different lines. The small colored dots represent the simulated centers of the single- and triple-point signatures, which are positioned in the middle of the bright scattering textures and demonstrate good consistency.

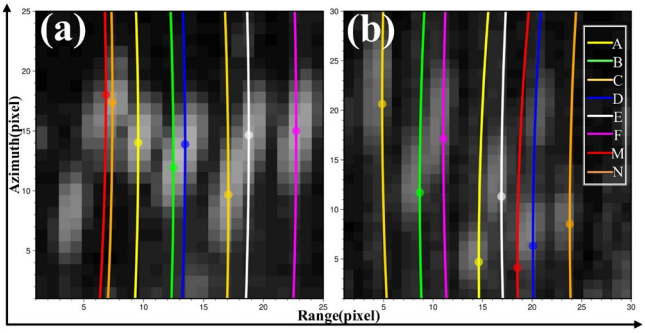

Fig. 6. Point signature simulations on an averaged SAR image (YZH). (a) Single-reflection; (b) Triple-reflection.

In the averaged SAR image, the bright scattering textures that are centered with single- and triple-point signatures are nearly 2 pixels wide in range and 10 pixels long in azimuth. The intensity of the single-reflection point signature in the averaged SAR image is nearly 10 dB higher than that of the triple-reflection point signature. In the range direction, the simulated lines and simulated points signature are nearly 0.5-pixel precision overlapped on the averaged point signature. In the azimuth direction, the simulated point signatures are 1~4 pixels.

B. Badong (Engshi, Hubei, China) case results

The second case is situated along Yangze River in Badong County, Enshi, China (BD). From 2019 to 2021, 48 TSX Spotlight mode images were collected and co-registered for subsequent analysis. The power lines are nearly 1200 m long and exhibit a slack catenary geometry, as depicted in Fig. 7a.

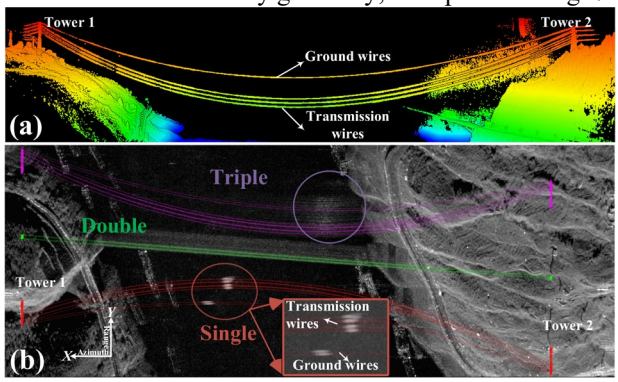

Fig. 7. Test site2, Badong, China. (a) Power line LiDAR data; (b) Simulated multi-reflection on the averaged image.

In Fig. 7b, the single-reflection point signatures are separated into two groups due to different catenary conditions of the transmission wires and ground wires. In contrast with the YZH case, double-reflection lines are visible in 92% of the SAR images. Triple-reflection effects in this scenario are always observed as line textures instead of point signatures. Fig. 7b shows that in the averaged SAR image, both double- and triple-reflection lines blur due to water level changes.

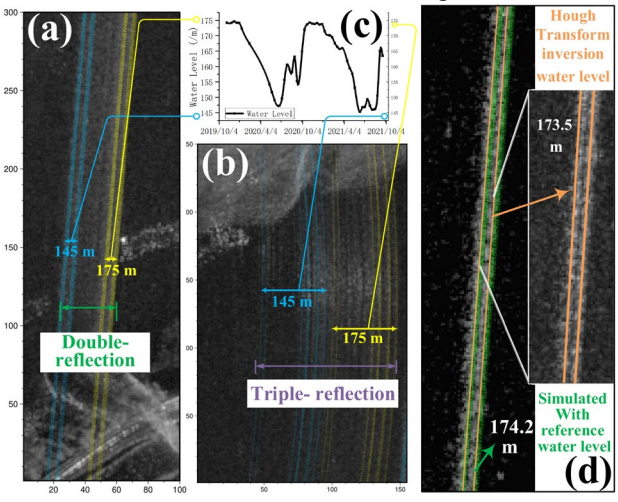

Fig. 8. Double- and triple-reflection textures of power lines in averaged TSX images. (a) Simulated double-reflection; (b) Simulated triple-reflection; (c) Water level changes; (d) Comparison of the water level derived from the proposed model with open-source data.

To illustrate the water level changes in Yangtze River in this area, Fig. 8 shows a partially enlarged averaged image with double- and triple-reflection textures. The yellow and blue arrows highlight the scattering textures for high (175 m) and low (145 m) water levels, respectively. Figs. 8a and 8b reveal that the triple reflection nearly doubled the range shift of the double reflection in response to the water level changes. Additionally, the notable double reflection in this case enables one to retrieve the water level of Yangtze River at this site. In Fig. 8d, the green dots represent the simulated double reflection based on open-source water level data at 174.2 m. The straight orange lines are derived from the Hough transform in [2] with an inversion water level of 173.5 m. The 0.7-m discrepancy is attributed to the inaccuracy of the reference water surface. Moreover, double-reflection textures occupy a certain range of pixels, whose inseparability also contributes to this discrepancy.

The simulated single-reflection lines and spot centers are consistent on the averaged image in Fig. 9a. The simulated lines have approximately 0.5-pixel precision in the range direction and 3~4-pixel precision in the azimuth direction.

Although the triple-reflection point signatures in this case are shown as a bright curved line texture, the simulated point signatures are located in the center of the bright curved-line texture. In Fig. 9a, the transmission wires have nearly 5 dB higher single-reflection intensity than the ground wires because they are 1~2 cm larger in line diameter than the ground wires. The triple-reflection intensity between these two types of wires is not as significant.

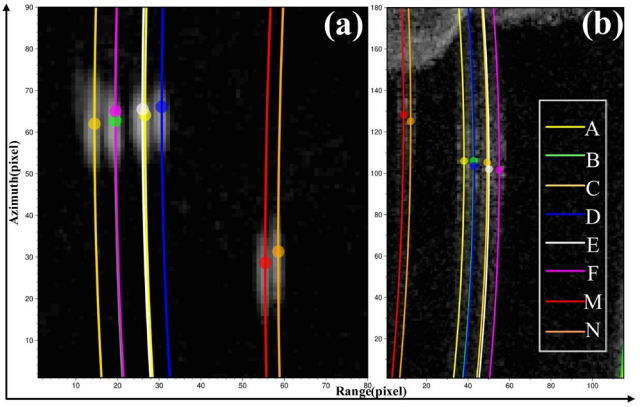

Fig. 9. Point signature simulations on an averaged SAR image (BD). (a) Single-reflection; (b) Triple-reflection.

V. Conclusion

This work analyzed the complex multi-reflection effects of the 2~3-cm-diameter cylinder metal power line over a water surface. The proposed point scattering tracing method enables us to explain the multi-reflection route passing through the water surface under the specular assumption. The single-reflection point signature comes from a certain segment of the power line. These segment centers can be identified in SAR coordinates via a quadratic polynomial model.

The power lines over the water surface have double-reflection, which is occasionally presented as a linear line texture, and triple reflection, which sometimes forms a curved-line texture or a point signature.

The ripples on the water surface appear to be a significant factor for the generation of double- and triple-reflection scattering. In the YZH case, where the lake water is calmer, nearly 50% of the reflections are double reflection. Double reflection occurs in 92% of the datasets in the BD case along the river with more ripples.

The Geometrical Optics (GO) method in this paper is effective in interpreting multi-reflection effects. However, it cannot fully explain the occasional disappearance of double and triple reflections. Factors such as the propagation parameters of creeping waves, rate and direction of power line swing, and state of water ripples may influence their occurrence. Quantifying these factors can help monitor the swinging condition of power lines.

Acknowledgment

This work was sponsored by the National Natural Science Foundation of China (Nos. 42074031, 41674032, and 41274048). TerraSAR-X data are copyright of German Aerospace Agency (DLR) and were provided via proposal motagh_GEO1916 and motagh_LAN3347.

References

[1] J.-S. Lee, E. Krogager, T. L. Ainsworth, and W.-M. Boerner, "Polarimetric Analysis of Radar Signature of a Manmade Structure," *IEEE Geosci. Remote Sensing Lett.*, vol. 3, no. 4, pp. 555–559, Oct. 2006.

[2] S.-W. Kim and Y.-K. Lee, "Accurate Water Level Measurement in the Bridge Using X-Band SAR," *IEEE Geosci. Remote Sensing Lett.*, vol. 19, pp. 1–5, 2022, doi: 10.1109/LGRS.2021.3138396.

[3] S. Auer, S. Hinz, and R. Bamler, "Ray-Tracing Simulation Techniques for Understanding High-Resolution SAR Images," *IEEE Trans. Geosci. Remote Sens.*, vol. 48, no. 3, pp. 1445–1456, Mar. 2010.

[4] M. Rebmeister, S. Auer, A. Schenk, and S. Hinz, "Geocoding of Ground-based SAR data for Infrastructure Objects Using the Maximum A Posteriori Estimation and Ray-tracing," *ISPRS J. Photogramm. Remote Sens.*, vol. 189, pp. 110–127, Jul. 2022.

[5] D. Brunner, G. Lemoine, H. Greidanus, and L. Bruzzone, "Radar Imaging Simulation for Urban Structures," *IEEE Geosci. Remote Sensing Lett.*, vol. 8, no. 1, pp. 68–72, Jan. 2011, doi: 10.1109/LGRS.2010.2051214.

[6] L. Yan, H. Ailing, L. Sha, L. Xingkai, W. Wenhao, and L. Tao, "High Voltage Power Line Scattering Feature Analysis in Multi SAR Sensors and Dual Polarization," in *Proc. 2nd Int. Workshop Earth Observ. Remote Sens. Appl. (EORSA)*, Jun. 2012, pp. *225–229*.

[7] L. Sha et al., "Study on extra-high voltage power line scatterers in time series SAR," in *Proc. 3rd Int. Workshop Earth Observ. Remote Sens. Appl. (EORSA)*, Jun. 2014, pp. 47–51, doi: 10.1109/EORSA.2014.6927847.

[8] K. Sarabandi and Moonsoo Park, "A Radar Cross-section Model for Power Lines at Millimeter-wave Frequencies," in *IEEE Trans. Antennas Propagat.*, vol. 51, no. 9, pp. 2353-2360, Sept. 2003.

[9] S. Shi, S. Wang, T. Li, Y. Liu, and H. Sun, "Numerical Simulation of the Radar Cross Section of UHV/EHV Power Lines Illuminated by X-, C-, L-, and P-Band Spaceborne SAR," *IEEE Trans. Geosci. Remote Sens.*, vol. 61, pp. 1–14, 2023, doi: 10.1109/TGRS.2023.3288516.

[10] L. Zhang and C. Liu, "Oil Tank Extraction Based on Joint-Spatial Saliency Analysis for Multiple SAR Images," *IEEE Geosci. Remote Sensing Lett.*, vol. 17, no. 6, pp. 998–1002, Jun. 2020, doi: 10.1109/LGRS.2019.2937355.

[11] C. Ma et al., "End-to-End Method with Transformer for 3-D Detection of Oil Tank from Single SAR Image," *IEEE Trans. Geosci. Remote Sens.*, vol. 60, pp. 1–19, 2022, doi: 10.1109/TGRS.2021.3127986.

[12] T. Mavridis, L. Petrillo, J. Sarrazin, D. Lautru, A. Benlarbi-Delai, and P. De Doncker, "Creeping Wave Model of Diffraction of an Obliquely Incident Plane Wave by a Circular Cylinder at 60 GHz," *IEEE Trans. Antennas Propagat.*, vol. 62, no. 3, pp. 1372–1377, Mar. 2014.

[13] E. F. Knott, "Phenomenological Examples of Radar Cross Section," in *Radar Cross Section*, Institution of Engineering and Technology, 2004, pp. 225–268. doi: 10.1049/SBRA026E_ch6.